Parameterization of urban characteristics for global climate modeling

Trisha L. Jackson[1], Johannes J. Feddema[1], Keith W. Oleson[2], Gordon B. Bonan[2], John T. Bauer[3]

[1]Department of Geography
University of Kansas
Lawrence, KS 66045
trish@ku.edu (Jackson)
feddema@ku.edu
785-864-5143
785-864-5378 fax

[2]National Center for Atmospheric Research
Climate and Global Dynamics Division
P.O. Box 3000
Boulder, CO 80307
oleson@ucar.edu
bonan@ucar.edu
303-497-1740
303-497-1314 fax

[3]Department of Geography
University of Nebraska – Kearney
Kearney, NE 68849
bauerjt@unk.edu
308-865-8682
308-865-8980 fax

Files:

Document:	tjackson_text.docx (includes coversheet, text, captions, references)
Captions:	tjackson_captions.docx (as requested by graphics guidelines)
Table:	tjackson_table.xls (very large and complex so not printed)
Figures:	tjackson_Figure01.tif
	tjackson_Figure02.tif
	tjackson_Figure03.tif
	tjackson_Figure04.tif
	tjackson_Figure05.tif
	tjackson_Figure06.eps
	tjackson_Figure07.tif
	tjackson_Figure08.tif
	tjackson_Figure09.tif
	tjackson_Figure10.tif
	tjackson_Figure11.tif

Acknowledgements

This research was partly supported by the National Center for Atmospheric Research Weather and Climate Impact Assessment Program and the Water System Program, National Science Foundation grants ATM-0107404 and ATM-0413540, and the University of Kansas, Center for Research. The National Center for Atmospheric Research is sponsored by the National Science Foundation.

Parameterization of urban characteristics for global climate modeling

Abstract

To help understand potential effects of urbanization on climates of varying scales and effects of climate change on urban populations, urbanization must be included in global climate models (GCMs). To properly capture the spatial variability in urban areas GCMs require global databases of urban extent and characteristics. This article describes methods and characteristics used to create a dataset that can be utilized to simulate urban systems on a global scale within GCMs. The dataset represents three main categories of urban properties: spatial extent, urban morphology, and thermal and radiative properties of building materials. Spatial extent of urban areas is derived from a population density dataset and calibrated within 33 regions of similar physical and social characteristics. For each region four classes of urbanization are identified and linked to a set of typical building morphology, thermal and radiative characteristics. In addition, urban extent is simulated back in time to 1750 based on national historical population and urbanization trends. A sample set of simulations shows that the urban characteristics do change urban heat island outcomes. In general the simulations show greater urban heat islands with increasing latitude, in agreement with observations.

Key Words: urban climate, climate simulation, urban properties, global climate change

Introduction

Beginning with observations of the London heat island in the late nineteenth century (Howard 1833) and subsequent observational evidence (Landsberg 1981), there is clear evidence that urban systems represent the greatest human impact on local climates. Further analysis of these systems shows that urban systems affect the radiation and energy balance in predictable ways that allows these impacts to be effectively simulated (Oke 1974; Arnfield 2000, 2003). In addition to modifying local climates, urban systems are also the primary interface between human activities and other human impacts on climate. For example, most anthropogenic emissions originate from urban areas and their peripheral regions (e.g. Decker et al. 2000; Mills 2007).

With the rapid growth of urban areas in modern society, it is likely that these urban systems will play an important role in human climate interactions in the future, thus they should be included as a component of the future global climate models (GCMs) (e.g. Oleson et al. 2008a). Incorporating urban systems within a GCM framework has two main reasons: first, to understand how urban areas might be contributing to climate change and the spatial distribution of emissions, and second, to learn how urban populations will be affected by climate change (Oleson et al. 2008a, 2008b) and to improve our understanding of urban climates on a global scale (Oleson et al., forthcoming). In addition, as governments work to address global warming, policymakers will first look at areas where most people reside, our cities. Using GCMs as a learning tool will help scientists test ideas and make recommendations about how to alter urban characteristics to lessen their impact on climate and energy consumption (Oleson, Bonan, and Feddema 2010). Additionally, if GCM projections show that urban responses to climate change

differ compared to the response in natural environments, it is important that this differential response be included in climate impact assessment studies.

Realizing a need for and justifying the need for global urban modeling is a first step. However, any global scale modeling effort requires that the model work for all places and in all seasons. In addition, spatial characteristics and physical properties of urban systems vary widely because of cultural factors and the differing sources of primary building materials (Grimmond and Souch 1994; Grimmond and Oke 1999; Grimmond 2007). This work addresses the need for a global urban dataset that provides urban spatial and physical properties that fulfill the parameter needs for modeling urban systems in GCMs. The three core parameterizations are: 1) spatial extent of urban areas, 2) urban morphology characteristics including building heights, urban canyon height-to-width ratios, plan area of buildings, impervious (e.g. sidewalks and roads) and pervious covers (e.g. parks and lawns), and 3) thermal and radiative properties of building and road materials (Oleson et al. 2008a). To illustrate the importance of these parameters we will present simulations showing differences in the global distribution of urban heat islands with different assumptions about urban system properties.

Background

Urban systems affect climate through a number of mechanisms that affect the absorption and disposition of energy because of 1) urban canyon geometry, 2) heat storage in building materials, 3) reduced evapotranspiration due to the increase in impervious cover and subsequent decrease in vegetation, and 4) the trapping of atmosphere-warming pollutants via temperature inversion (Oke 1982; Oke 1987; Oke et al. 1991).

Theoretical and satellite studies highlight the urban characteristics that result in urban climate modification, most often expressed as urban heat islands. First, the size, shape, and orientation of physical components, or urban morphology, explain in part the temperature contrast with adjoining rural areas. Additional alteration of the urban surface response depends on physical properties of these factors. These physical properties are subdivided into thermal properties (i.e. heat capacity, thermal conductivity) and radiative properties (i.e. emissivity, albedo), which combine to account for temperature differences. The combined morphology and physical properties of urban areas explain the differential radiation balance at the surface compared to surrounding rural areas. Moreover, these factors account for storage of heat in urban materials and the partitioning of energy into latent and sensible heat fluxes (Landsberg 1981; Oke 1982, 1987, 1988, 1995). Because of the complexity of these interactions, urban climate modelers face many challenges, particularly when working at the global scale.

Several advances of modeling theory of urban-climate interactions have occurred since Oke (1974) published an initial review of urban climatology. From that point forward, modelers began considering individual buildings, including wall and roof facets, each experiencing varying time exposure of solar radiation, net longwave radiation exchange, and ventilation (Arnfield 1984, 2000; Paterson and Apelt 1989; Verseghy and Munro 1989a, 1989b). The

horizontal aspect of urban systems contains impervious (e.g. paved roadways) and pervious surfaces (e.g. lawns) with different properties and interactions including radiative, thermal, aerodynamic, and hydrological elements (Oke 1979; Suckling 1980; Doll, Ching, and Kaneshiro 1985; Asaeda, Ca, and Wake 1996; Anandakumar 1999; Oke 1989; Grimmond, Souch, and Hubble 1996; Kjelgren and Montague 1998). These horizontal surfaces along with walls of buildings define the urban canyon (Figure 1). This fundamental morphological urban unit can be scaled up to encompass the area needed for a particular model, from a city block to an entire city.

Previous modeling approaches include detailed mapping of urban morphology (Ellefsen 1990-91; Grimmond and Souch 1994; Cionco and Ellefsen 1998) or direct observation of urban systems at aggregate scales, such as the objective hysteresis model by Grimmond, Cleugh, and Oke (1991) and mesoscale modeling to study interactions between urban systems and local weather patterns (Changnon 1992; Shepard 2005). Other models have used the urban canyon concept to incorporate joint interactions of the combined budgets of component facets (Terjung and O'Rourke 1980a, 1980b; Mills 1993; Arnfield 2000; Masson 2000). Development of the parameter set in this study is intended for use with such urban canyon type models, but can be modified to meet the need of other modeling strategies.

A number of factors must be considered when designing a model that operates on a global scale including computational efficiency and its ability to simulate urban systems in a wide variety of climates (Oleson et al. 2008a). However, the response of urban systems will differ geographically based on the properties related to urban design and building materials used. These characteristics must be documented in order for a global model to effectively simulate urban responses to climate change. In addition, these characteristics must be able to change over time to better assess the impact of climate change on urban populations, which includes more

than half of the total world population today and is projected to include about 65-70 percent of the global population by 2050 (CIESIN et al. 2004; Shepherd 2005).

The dataset described here was developed to correspond with requirements of the National Center for Atmospheric Research's (NCAR) urban sub-model (CLMU; Oleson et al. 2008a, 2008b). CLMU is a sub-model of the Community Land Model (CLM; Oleson et al. 2008c) of the Community Climate System Model (CCSM; Collins et al. 2006). In the upcoming CCSM 4.0, the Earth's surface is divided into grid cells approximately at one degree resolution. To characterize the varied landscapes that occur within a grid cell at this resolution, each grid cell has the capacity to be unique. A CLM grid cell consists of a nested sub-grid hierarchy including land units, plant functional types (PFTs), and snow/soil columns (Oleson et al. 2004). Presently, the CLM contains five land unit types of glacier, wetland, lake, vegetation, and for version 4.0, urban. Of the five land unit types, only vegetation and urban classes can be further subdivided. Vegetation is divided into PFTs while the urban area subdivided into five urban facets, sunlit and shaded walls, roofs, impervious surfaces (roads) and pervious areas in the canyon floor (Figure 2). The full description of the model's design and sensitivity tests can be found in Oleson et al. (2008a, 2008b).

CLMU simulates six main energy balance processes: 1) absorption and reflection of solar radiation, 2) absorption, reflection, and emission of longwave radiation, 3) momentum, storage, sensible, and latent heat fluxes, 4) anthropogenic heat fluxes due to waste heat from building heating/air conditioning, 5) heat transfer in roofs, building walls, and roads, and 6) hydrology (Oleson et al. 2008a). The urban model calls for morphologic, thermal, and radiative input parameters to efficiently simulate these processes. Urban canyon morphology is captured by urban canyon height-to-width ratio, average building height, roof fraction (as a percent of total

area), pervious and impervious canyon floor fractions, roof and wall thicknesses, and impervious canyon floor thickness. Thermal parameters include thermal conductivity and volumetric heat capacity for roofs, walls, impervious and pervious canyon floor materials, minimum and maximum interior building temperatures, and soils of differing textures. Radiative properties are emissivity and albedo of roofs, walls, and impervious and pervious canyon floor materials.

This detailed information provided to the model aids in capturing the character of an urban area. Considering that cities across the world vary widely in terms of structure (i.e. different canyon widths, different building heights) and building materials, these parameters successfully portray the dissimilarities from region to region and between urban categories (e.g. tall building districts versus low density residential areas).

Methodology

A three-step process was employed to complete the urban dataset. Initially, the Earth's land surfaces were divided into manageable regions with similar urban character. Next, spatial extent of four categories of urban intensity was determined, and finally, a database of building and road properties for each regional category was compiled.

To better manage the information at a global scale we divided the world into regions. With generalization of regions, an initial dataset can be completed in a timely manner to provide a framework that allows for future improvements in the detail of the data. Therefore, the division of the globe into regions with similar urban character was our first step (Figure 3). In making these generalizations, physical and cultural geography played a significant role, as well as the realization that for many regions this information is difficult to obtain, limiting our ability to further subdivide areas that we realize are not necessarily homogenous in political or even building characteristics. Thus the overriding criteria is based on the fact that , buildings are designed to withstand weather conditions of an area, so climate was a one determinant, as well as available resources for building materials (Givoni 1976; Olgyay 1992) in discerning regional boundaries. Culture also plays a role in the structure of buildings and cities (Clarke 1989).

For this study we evaluated each of the 33 regions (Figure 3) to determine unique urban-rural boundaries and then to delineate between four levels of urban intensity based on population density. Population density proved to be the most reliable proxy for urban intensity after several satellite-derived landcover products were evaluated for defining urban extent (e.g. MODIS, GLC2000, and DISCover). Not only do these products show significant disagreement on the location and size of urban areas, but they also do not provide levels of urban intensity, which is a required parameter of CLMU. Population density as provided by LandScan already considers

slope, landcover, nighttime lights, proximity to roadways, and census data to determine where people are most likely living (Dobson et al. 2000). Population density is not a perfect determinant of urban concentration, but it provides an easy transition to temporal usage so it offers the ability to answer more questions than a satellite based snap-shot of urban areas. With emergence of new population datasets, the time series of population densities lengthens, assisting in the study of urban evolution over time.

Using LandScan 2004 population densities (ORNL 2005), a lower limit of population density for each region was selected to define the urban-rural boundary. Once urban areas were defined, they were further delineated into four levels of urban intensity, including tall building district (TBD), high density (HD), medium density (MD), and low density (LD). Population density boundaries for each of these urban levels differ widely to account for different types of urban communities. For example, East Africa contains many small farm plots housing large families. This causes the population density to be relatively high for an agriculture-based community, and it has many characteristics of for example U.S. suburbs, such as low buildings and a high percentage of green space.

Intra-urban boundaries (e.g. between low and medium density) were based on population density and observations of satellite imagery in at least ten sample cities per region (i.e. validation cities). Validation cities were chosen based on size (i.e. large urban population), location (i.e. to geographically represent the entire region), and best available resolution of satellite imagery in Google Earth. The images in Google Earth come from a variety of sources (e.g. TerraMetrics, NASA, DigitalGlobe), and the available resolutions vary as well, from 15m in most cases (EarthSat 2007) to less than one meter (DigitalGlobe 2007). During comparisons of LandScan population density (Dobsen et al. 2000) to satellite images natural boundaries

typically presented themselves in the form of a relatively large disparity of neighboring LandScan pixels corresponding to a change in urban land surface properties (e.g. vegetated fraction, building density, etc.) as seen in Google Earth.

For each region, boundaries were assigned based on an initial validation city, then adjusted for each subsequent validation city. The initial cities were then re-checked to assure the adjustments still properly represented their intra-urban boundaries.

To maintain consistency from region to region during this process, definitions for the urban categories were established from the start. Tall building districts (TBD) here are defined as an area of at least 1 km^2 with buildings greater than or equal to 10 stories tall, with a small fraction of vegetation (i.e. 5-15 percent of plan area). Many cities that may appear to have a TBD were not included in this dataset because the aerial extent was too small (i.e. less than 1 km^2) or because the population density of the TBD was too sparse. High density (HD) areas may encompass commercial, residential, or industrial areas and are characterized by buildings 3-10 stories tall with a vegetated/pervious fraction typically in the range of 5-25 percent. Medium density (MD) areas are usually characterized by row houses or apartment complexes 1-3 stories tall with a vegetated/pervious fraction of 20-60 percent. Finally, the low density (LD) category covers areas with 1-2 story buildings and a vegetated/pervious fraction of 50-85 percent. LD includes a variety of urban types, from the suburbs of the United States to urban agricultural parts of East Africa.

As a final step in defining urban extent, an inter-region comparison looked at disparities on the global scale such as population percentile rank of each boundary. This ensured that regions with similar qualities were consistent in their assignment of urban categories. In this process,

minor adjustments were made to the urban-rural and intra-urban boundaries to maintain consistency in urban levels from region to region.

Upon further evaluation we concluded that only TBD, HD and MD urban types can be adequately simulated in the CLMU. This decision is based on the fact that in suburban or high population density agricultural areas the assumptions about radiation trapping and aerodynamic processes in the urban canyon model do not hold true when vegetation is a dominant component of the landscape. We propose to develop a separate suburban model in the future to properly handle such landscapes. Thus for the purpose of global models only the TBD, HD and MD classes should generally be used to simulate urban systems in an urban canyon type model. The intra-urban categories (TBD, HD, MD, and LD) must be adaptable to any location. For example, LD encompasses suburbs in the United States and urban-agriculture in East Africa, and similar differences exist for the other urban classes. For the model to delineate between places that fall within the same category, additional information is required for the buildings and surrounding area at each locale. Therefore we define urban morphology characteristics for each of the 132 regional categories (i.e. 33 regions x 4 categories) including average building heights (H), urban canyon height-to-width ratios (H:W), and fraction of pervious surface (*e.g.* vegetation), roof area, and impervious surfaces (e.g. roads and sidewalks). In this article we summarize our methods, but precise values and references for each measurement are presented in the database provided as supplemental material to this paper.

To estimate average building heights for the validation cities, a global database of tallest buildings by cities was used for TBDs within each region (Emporis Corporation 2007). Where available, the 25 tallest buildings were averaged for five cities within a region, then the average building heights of these cities were calculated to determine an average regional tall building

value. This average was then decreased proportionately to account for the remaining buildings in the TBD resulting in an average TBD building height representative of each regional category. In regions with no TBD (e.g. Greenland), or those with few cities with a TBD (e.g. West Africa), the maximum number of buildings in the buildings database was used in the calculation.

For the HD category, Emporis Corporation (2007) data were used where available and were supplemented by imagery of verification cities. By studying imagery of city skylines, building heights could be estimated by comparing TBD heights to HD buildings. To further aid the estimation process, the number of stories of HD buildings was counted in order to approximate heights. For the remaining categories of MD and LD, building heights were determined based primarily on dominant housing types. For instance, a typical two-story frame home in the U.S. is approximately eight meters tall. References to local building codes and estimations from imagery supplement this method. Further, since part of the dataset presented here includes typical building types for each category, the gathering of this information also helped resolve typical building heights.

Local building codes and other municipal documentation were also used to ascertain road widths and other required information (e.g. lawn area) for calculation of H:W ratios of representative urban canyons. Where official documentation was absent, road widths were found on the internet, usually as part of information necessary for emergency planners and other government agencies. Once road widths were known and additional canyon floor lengths (e.g. lawns, sidewalks) were estimated based on imagery or municipal documentation, H:W could be calculated with building heights for each regional category. To illustrate, consider a suburban area with 8m tall homes with a 24m canyon floor (including roads and lawns); the H:W equals 0.33 (i.e. 8m / 24m = 0.33).

Urban morphology also includes fraction of pervious (e.g. vegetation), roof area, and impervious area (e.g. roads and sidewalks). Imagery from Google Earth for each regional category's validation cities provided the primary tool for estimating these fractions. In essence, the spatial extent dataset was used to identify a cluster of pixels within a validation city for the desired urban category (i.e. TBD, HD, MD, LD). Then the location was identified in the satellite imagery and studied (which often involved using the distance measuring tool to calculate actual plan area) before an estimation of these fractions was assigned. Percent pervious and roof area were initially estimated, and then percent impervious could be deduced based on this information. Since the majority of impervious surfaces in urban areas are roadways, it is considered to be the road fraction in the model input.

Urban morphology considers the three-dimensional form of the urban canyon, but additional information on thermal and radiative properties of building materials are required to effectively capture urban interaction with climate at many scales (Bonan 2002). The primary reason for distinguishing building types is to promote the model's ability to simulate thermal and radiative exchanges within the urban canyon. Buildings are the main component of the urban canyon, especially in terms of how their structure and materials influence the canyon's thermal storage and radiative balance. Therefore, a database of typical building types and their associated properties was compiled.

By studying imagery, construction data by country, and/or other published documentation on building types and housing for every region (e.g. Canada's National Research Council Institute for Research in Construction), a list of the most common building types in the world was assembled. For the 132 regional categories, the three most common building types and roof types were determined and their relative abundance was reported in percentage terms (e.g. Walls:

50 percent wood frame home, 40 percent brick home, 10 percent stone home; Roofs: 70 percent asphalt shingle, 20 percent ceramic tile and 10 percent wood shingle). Learning what constitutes common building and roof types involved background research in building trade literature as well as studying documentation describing historical and cultural determinants of typical buildings in a region today and in the recent past (Givoni 1976; Olgyay 1992; Straube and Burnett 2005). However, there were many cases in which imagery and geographical knowledge played a large role in approximating the most common building and roof types as well as establishing the primary road type found in each category.

Establishing common wall, roof, and road types laid the groundwork for ascertaining their individual makeup as represented by portioning walls and roof into discrete layers. With each building type there was a typical method of construction, or a way of assembling walls. Once the order of the construction materials was ascertained, each respective wall or roof type was divided into ten layers with information on each layer's thickness (Oleson et al. 2008a). The road types were limited to the number of actual layers present; subsequent layers are occupied by soil.

In a wall or roof with fewer than ten actual layers of materials, each material may occupy more than one layer in a row to satisfy model requirements. For instance, one building type is "mud or adobe." Since mud is the only wall material, mud was stated as the material for every layer and the sum of individual layer thicknesses equals the standard thickness of a mud or adobe home. Thus by determining common construction techniques for different types, a list of typical building materials divided into ten layers could be established for each wall and roof type (see the supplemental Excel file).

Next, thermal and radiative properties were collected for each construction material including density, specific heat capacity, and thermal conductivity. Only for surface materials were albedo and emissivity values collected. CLMU calls for volumetric heat capacity (Oleson et al. 2008a), which was calculated using density and specific heat capacity where necessary. The compiled lookup table of material thermal and radiative values was used; the literature sources of the values are presented in the supplemental materials. A final calculation was the summation of total wall thickness. The entire process was repeated for roofs and roads. The result was a database of typical wall, roof, and road types with associated thermal properties by layer and radiative properties of surface layers. Based on this background, a table of three wall types, three roof types, their relative abundances and one road type was constructed for each regional category.

At present, CLMU can accommodate only one urban class, and only one set of representative thermal and radiative properties within the TBD, HD, and MD categories can be used. The class selected is based on which is most abundant in a GCM grid cell, and the values are comprised of weighted averages of the three typical wall and roof types within that class. To arrive at these representative values, a first step is to calculate whole-wall thermal conductivity, which requires that the values must be converted to thermal resistance (i.e. R-value), an additive property. Thermal conductivity is conceptually and mathematically related to thermal resistance by dividing the wall layer width by its thermal conductivity. R-values of the 10 layers are then summed to arrive at a whole-wall (or whole-roof) R-value for each type. This value is divided by its respective wall or roof width to arrive at the whole-wall or whole-roof thermal conductivity. Calculating R-values for the whole wall or roof allowed comparison of these values to published estimates of these values. Since the published values show that walls in

reality are much less thermally efficient compared to the theoretical values associated with the layers of materials that make up a wall, we must consider sources of heat transfer. For instance, we calculated R-values in series for some walls (i.e. mud or adobe) since the wall is consistent throughout (i.e. the layers are in series), and calculated R-values in parallel for other walls (i.e. wood frame walls) to help account for thermal differences in layers that occur in parallel (i.e. in the same lateral space; for example, windows in a wall).

Another important consideration in developing a dataset of thermal building properties that represents the real world is to consider thermal bridging and air leakage. Thermal bridging initiates heat transfer through materials where there is a discontinuity in the insulation or construction material (e.g. staples or nails used to hold insulation in place, wood or steel columns in a wall, internal corners of walls, floors, and ceilings, etc.). Thermal bridging along with air leakage (e.g. from chimneys, windows, doors, porous building materials such as brick, joints between materials, etc.) causes buildings to be less thermally efficient.

To account for the majority of thermal inefficiencies of buildings, which are poorly documented and known to vary from region to region and within regions (Rashkin et al. 2008), total wall resistance was multiplied by a factor of 0.2 for buildings with windows based on published estimates of typical resistance losses and estimates which suggest that windows account for 22-37 percent of total heat loss and occupy 15-40 percent of wall area (Rashkin et al. 2008). Roofs and glass curtain and corrugated iron walls were excluded from this adjustment since roofs have no windows and glass curtain walls are comprised almost wholly of windows, so their thermal properties already account for this, and corrugated iron walls typically have no windows.

Using these whole-wall or whole-roof thermal conductivities, along with the other thermal and radiative values (i.e. volumetric heat capacity, emissivity, and albedo), weighted average thermal values were calculated for TBD, HD, and MD regional categories to arrive at representative values considering the three main building types. For example, if three wall and roof types in a given category are weighted at 40, 30 and 30 percent, then their respective properties are also weighted in this way to arrive at one representative value. This value represents the weighted average properties of the typical wall or roof in a given category. Only one road type was listed for each category, eliminating the need for calculating averages.

A final step in preparing the urban properties database for CLMU was to provide estimates of temperature ranges for building interiors for the 132 urban categories. These general estimates are based on seasonal temperature averages and extremes, and a subjective evaluation of availability of heating and cooling methods (i.e. prominence of air conditioning).

The final product includes a GIS-based global dataset of urban extent divided into four urban categories. The 1-km resolution dataset is in geographical grid format. For use in the CCSM, data are also aggregated to a half degree grid (i.e. the 0.05 degree resolution data is summed by class to 0.5 degree aggregates), and, based on historical population estimates and histories of urbanization by region, we have extrapolated urban extent back to 1750. Associated data tables can be linked to the urban extent grid via region names. Tables included are: wall types, roof types, road types, material properties, percent of pervious and roof areas, thermal bridging and insulation calculations, a master table of three common building and roof types with their relative frequency as well as road types and internal temperature ranges per regional category.

Evaluation of the dataset

To explore the importance of spatially explicit urban characteristics we performed two uncoupled global CLM simulations at T42 resolution (~2.8° longitude by 2.8° latitude). The simulations were driven by a 57-year (1948–2004) atmospheric forcing data set from *Qian et al.* (2006). In other words, the climate conditions (radiation, precipitation etc.) were held constant for both experiments. In the control experiment we summed global regional areas of TBD, HD and MD to create an urban extent and applied the properties described by Voogt and Grimmond (2000) for Vancouver, B.C. to all urban areas. Building interior temperatures were maintained between 288.72 and 299.83ºK; however we did not implement the model function that includes expelling waste heat from heating and air conditioning back into the urban canyon (Oleson et al. 2008a). In a second experimental simulation we assumed the same urban extent, but applied the regional urban properties associated with the urban class (TBD/HD/MD) that represented the largest urban area in the grid cell. Because unintended interactions can occur when mixing properties of different urban classes only one class' properties should be used in an analysis. Analysis of the simulations is based on an evaluation of the heat island as measured by the difference between 1984-2004 climatologies of the urban reference height temperatures in a grid cell minus the average rural (the vegetation and soil fraction areas in the grid cell) reference height temperature. For those interested how other variables are simulated by the model, please refer to a more detailed analysis of model responses in Oleson et al. (forthcoming). In our analysis, observations are only shown for grid cells with urban extent.

Results and Discussion

Most striking about the final dataset presented here is the stark differences in urban characteristics from place to place, whether looking at the form of cities, the materials they are built from, or the density of the populations living there. Spatial extent shows variations in the form of cities, such as the dense, concentric ring form of older cities such as Paris, France and London, England (Figure 4) contrasted against most U.S. cities, which sprawl to cover large areas (Figure 5). Urban morphology displays another aspect of this contrast, with modern cities teeming with skyscrapers resulting in very high urban canyon height-to-width ratios versus the shorter, denser TBDs in places like India.

For the CLM simulation only the TBD, HD and MD urban extent were used. We extrapolated these areal extents backwards in time to 1750 using historical national population estimates and our own estimates of urbanization (Figure 6). It is also possible to compare our estimate of present day urban area for these three classes against existing data from the HYDE 3.0 (Klein Goldewijk 2006) dataset (Figure 7). The HYDE 3.0 urban areas are largely based in United Nations defined urban areas, which vary from country to country. Hence we see large differences in the datasets, with the U.S. showing less urban area in our dataset because we omitted the suburban class, and regions like India and China being more urban in our data because our dataset aggregates relatively small but high frequency urban centers like villages that show high population densities in the LandScan 2004 dataset.

Urban spatial extent and morphological parameters effectively capture visible differences in urban areas, while thermal and radiative properties capture less apparent, yet sharp contrasts between regions. A summary of estimated median, quartile and ranges for each parameter are summarized over the 33 regions (Figure 8) including published values for two test sites used to

validate the model (see Oleson et al. 2008a). Take for instance average thermal conductivity for typical wall materials for each region in the middle density category (Figure 9). The figure is presented in such a way to display a wall's insulating capability. Note that many low latitude regions contain walls that function as poor to extremely poor insulators, an effective adaptation for warm climates. On the contrary, there is no apparent latitudinal pattern associated with albedo of roof surfaces in low density areas (Figure 10a). However, Australia's effort to increase usage of roof materials with high albedo is apparent (Salhani 2009). Using highly reflective roofs or other less conventional materials for roof cover (e.g. grass) is a topic receiving a great amount of attention in the U.S. and other countries as a way of mitigating the urban heat island effect (Rashkin et al. 2008). CLMU has the capability to measure the effects of these types of changes on the atmosphere, which will be useful to policymakers, builders, and other stakeholders with the common goal of creating more efficient cities (e.g. Oleson, Bonan and Feddema 2010).

The final CLM input dataset differs slightly from the data presented in the supplementary materials because in each grid cell the CLM selected the properties associated with the most abundant urban type. For comparison we show the albedo for a single LD urban class (Figure 10a), which can be compared to the input for roof albedo as implemented in the model (Figure 10b).

Our model simulations show that whether using the Vancouver (Figure 11) or the dataset parameterization (Figure 11) we simulate effective heat island trends across the globe, with tropical areas typically having lower heat island impacts compared to higher latitude regions where more energy is added to the system to maintain building temperatures (for more details on the complete model response please refer to Oleson et al., forthcoming). Yet, there are also

significant differences between the Vancouver simulation and the parameter dataset simulation. Differences in wall and roof thermal and radiative properties and interior temperature settings result in tropical heat islands being significantly lower, typically about 0.5ºK, when using the new parameters compared to a typical Vancouver building structure in the same location. Heat islands increase by a maximum of about 1ºK in parts of Eurasia primarily because of different wall and roof properties and use of home heating.

As with any first effort of building a global database, there are issues and limitations associated with the process and with the proper use of the data. The primary concern in constructing a database of this scope was to identify methods resulting in a meaningful outcome. Although some data exist on urban extent and building materials, none have uniform global coverage. The methods employed here are, to an extent, arbitrary. At the same time, we must consider that this is a first attempt at characterizing a complex system on a global scale.

Using population density as a proxy to determine urban boundaries also presents issues when attempting to include urban areas such as industrial complexes and airports. With sparse population in these pixels, they often are either classified as rural, or the population of surrounding areas captures the district as low density. Although low density may be a suitable classification for airports, it does not properly describe the properties of industrial complexes. The urban spatial extent requires further development to enhance coverage of these sparsely populated sites.

Determining spatial extent was likely the most straight-forward process, but it was certainly not the simplest. After initially having only three classes of urban (Jackson 2007), there was too large a disparity between the qualities of low density urban across regional boundaries. Thus, the medium density class was added, and low density was reserved to describe suburban settings

and areas employing urban agriculture, which have a relatively dense population, but with a large fraction of vegetation. Because of the large fraction of vegetation in this class, it will be excluded from use in CLMU, although it will likely be used in future suburban models and useful for improving global landcover datasets.

Another challenge involved the classification of tall building districts. In the U.S., for example, the densest population areas are usually found adjacent to actual TBDs. Therefore, the location of TBDs in the dataset may not be precise, as most effort was put towards resolving the proper extent of the TBD for the region. We erred on the conservative side here, as for a given region top population densities varied from city to city, creating challenges in finding the middle ground. But since the dataset was to be scaled up to a half-degree resolution, accurate representation of the actual location for any given TBD is not a vital concern. Such errors can hopefully be corrected as additional information on urban areas becomes available in the future (e.g. Schneider, Friedl, and Potere 2009).

The urban spatial extent dataset has a resolution of 1 km, which, considering the scale of the project, allows a reasonable level of generalization. LandScan also has a resolution of 1 km, so the method outlined here can be repeated for later versions of LandScan. Furthermore, since the intended use of the dataset is to represent urban systems in GCMs with a grid resolution on the order of at least 50 km, the 1 km resolution is sufficient to serve this purpose. Yet if a user of the dataset wished to use the dataset for higher resolution studies, users must first consider if the dataset is accurate enough for meaningful representations at smaller scales.

The scale limitation also exists for the building characteristics data. Three building types were described for each regional category, which reasonably describes the overall character of a place. Even more importantly, three building types are sufficient to point out contrasting

elements between regions. Again, the database is suitable for global studies, but it is unlikely to be appropriate at smaller scales without addition of more detail. In addition to providing reasonable descriptions of building characteristics, the results also show a realistic simulation of heat islands which qualitatively agree well with observed heat island characteristics on a global scale (i.e. lower heat islands in the tropics and higher in high latitudes; also see Oleson et al., forthcoming).

Future work

As described throughout this article, urban areas across the globe vary greatly. Tall building districts in Japan and Australia tower over those found in India and South Africa. Housing varies from sophisticated, wood frame walls with solar panel roofs to simple mud huts with thatch roofs. In some places, extensive, manicured lawns are the norm, while elsewhere, grounds surrounding homes are cultivated for food. This dataset effectively captures these variances, and, at the same time, invites improvement. As the first of its kind, the urban dataset presented here is far from a final product. It is the hope of the authors that the dataset will be viewed and used as a living document. This dataset was created with the idea that it can be added to over time and to invite a wide ranging participation from other researchers to fill in areas presently lacking in detail. Using this project as a starting point, it would be fairly simple to further segregate regions or to add to or improve the precision of the data that is already present. The format of the database allows for progressive expansion of the data, and its design allows for scale modification to make it suitable for local or regional studies. The full dataset described here is available as a supplement to this publication and GCM ready versions at half degree grid resolution will be available on NCAR's website.

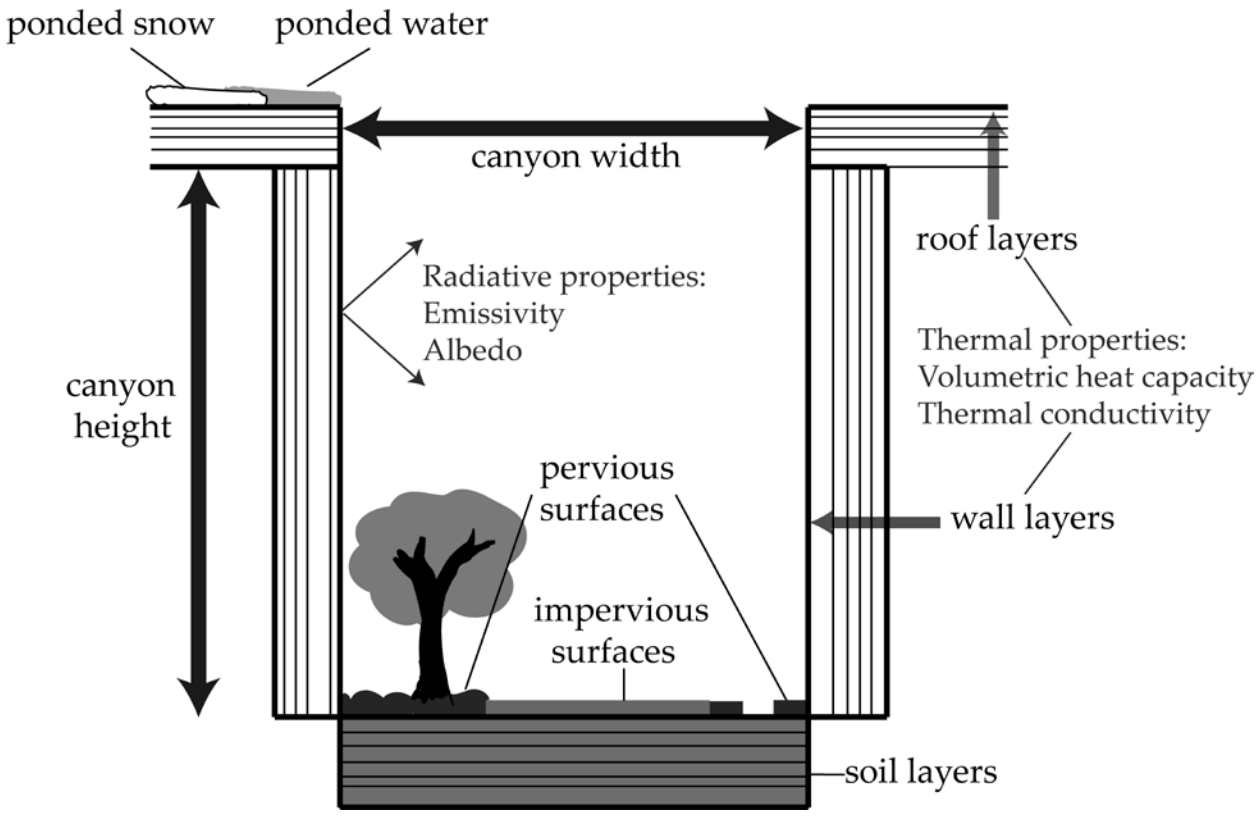

Figure 1. CLMU parameter requirements as discerned by the urban canyon concept.

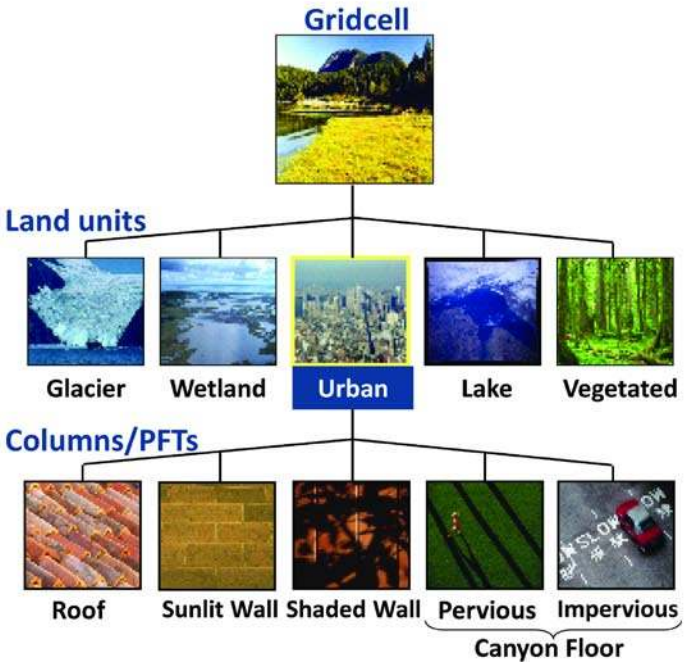

Figure 2. Schematic representation of the make-up of a typical CLM grid cell. The urban component is broken up into five facets to calculate the exchange of energy between the surfaces and the urban canyon.

Figure 3. Thirty-three regions with similar urban character. Delineating factors include climate and housing characteristics.

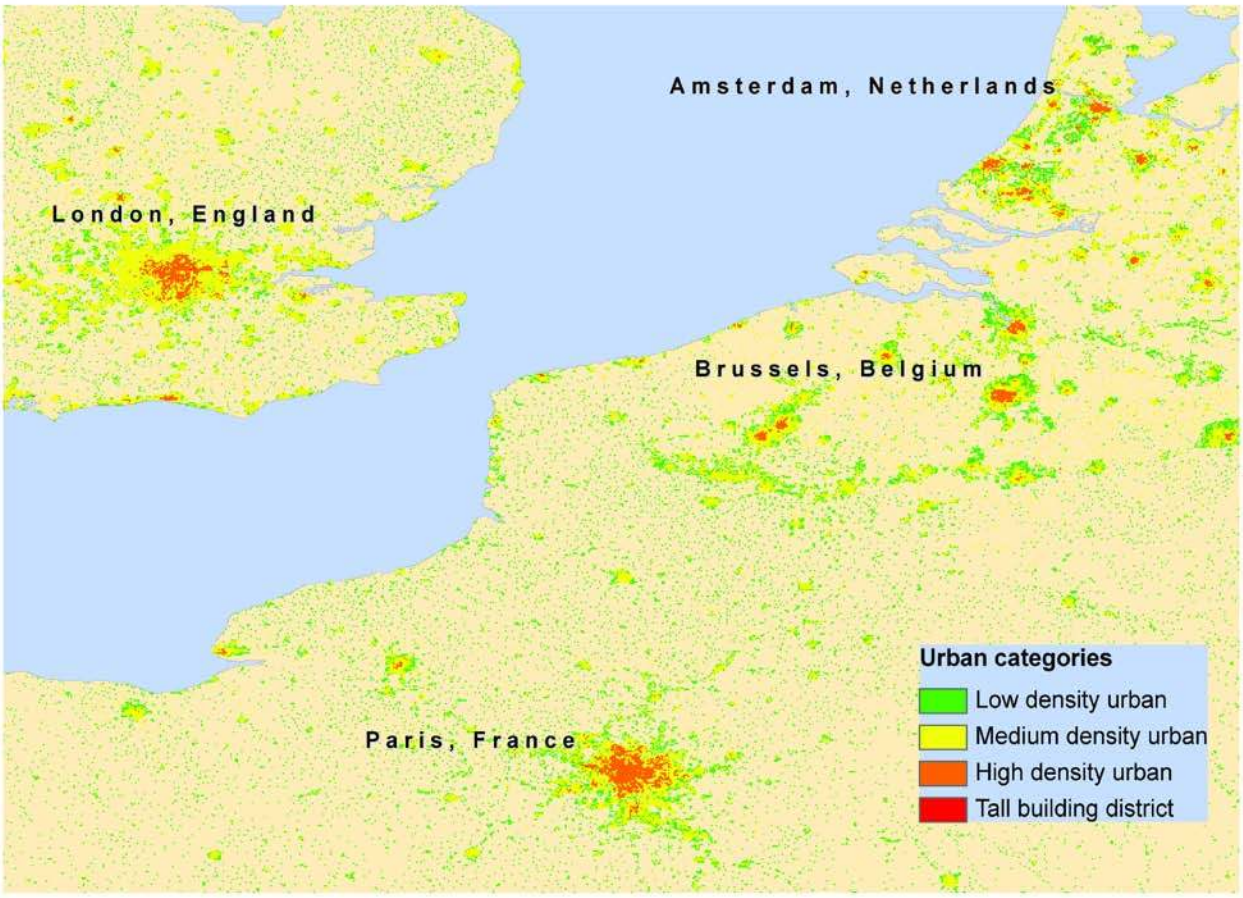

Figure 4. Urban areas, by category, of western Europe. One pixel represents about one kilometer.

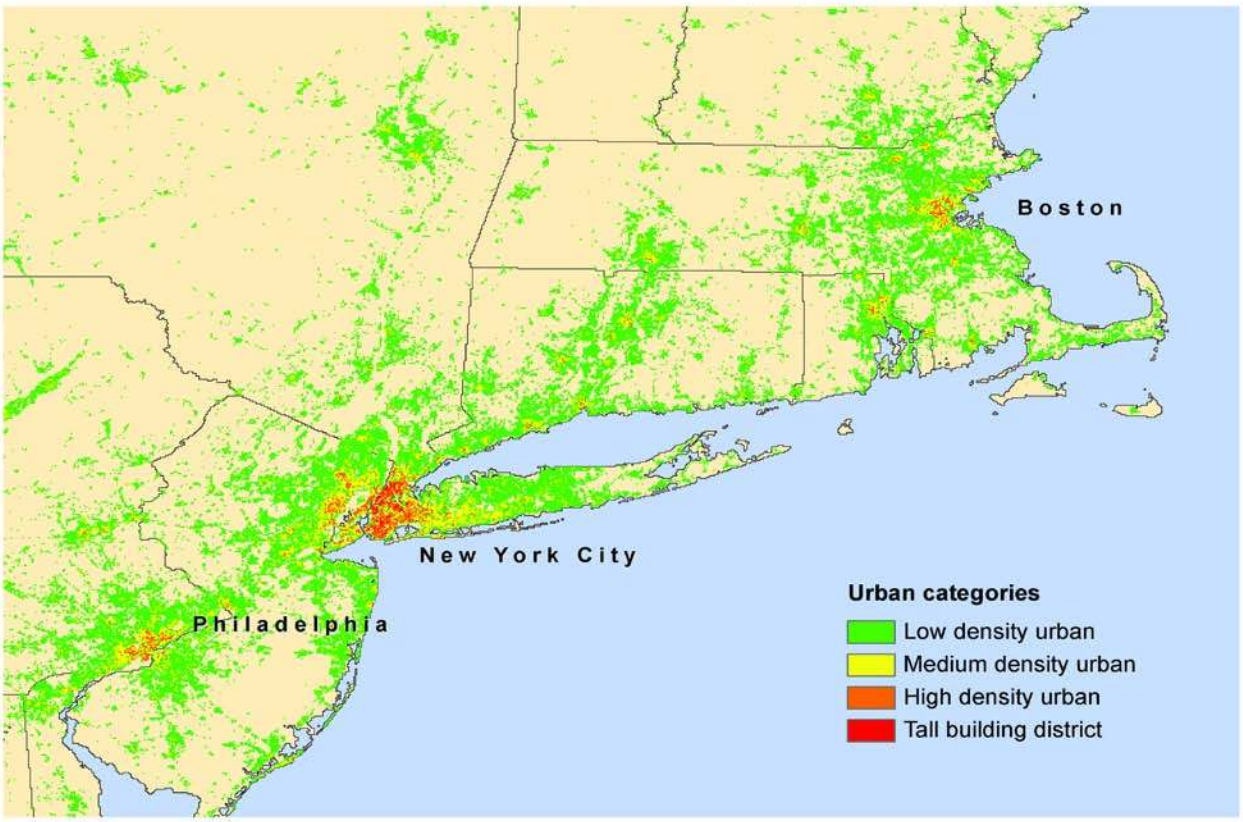

Figure 5. Urban areas, by category, of the northeast United States. One pixel represents about one kilometer.

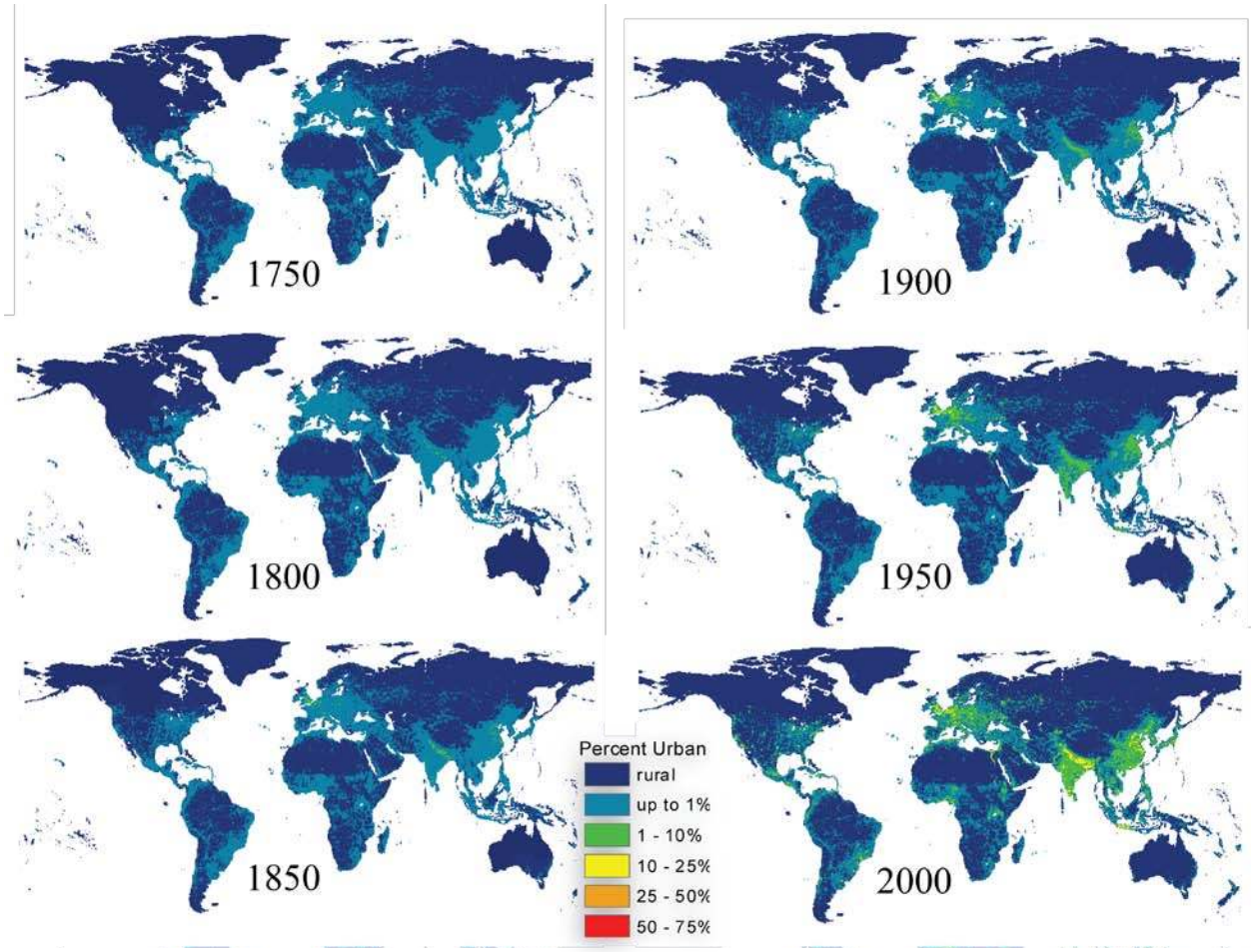

Figure 6. Global estimates of urban extent from 1750 to present.

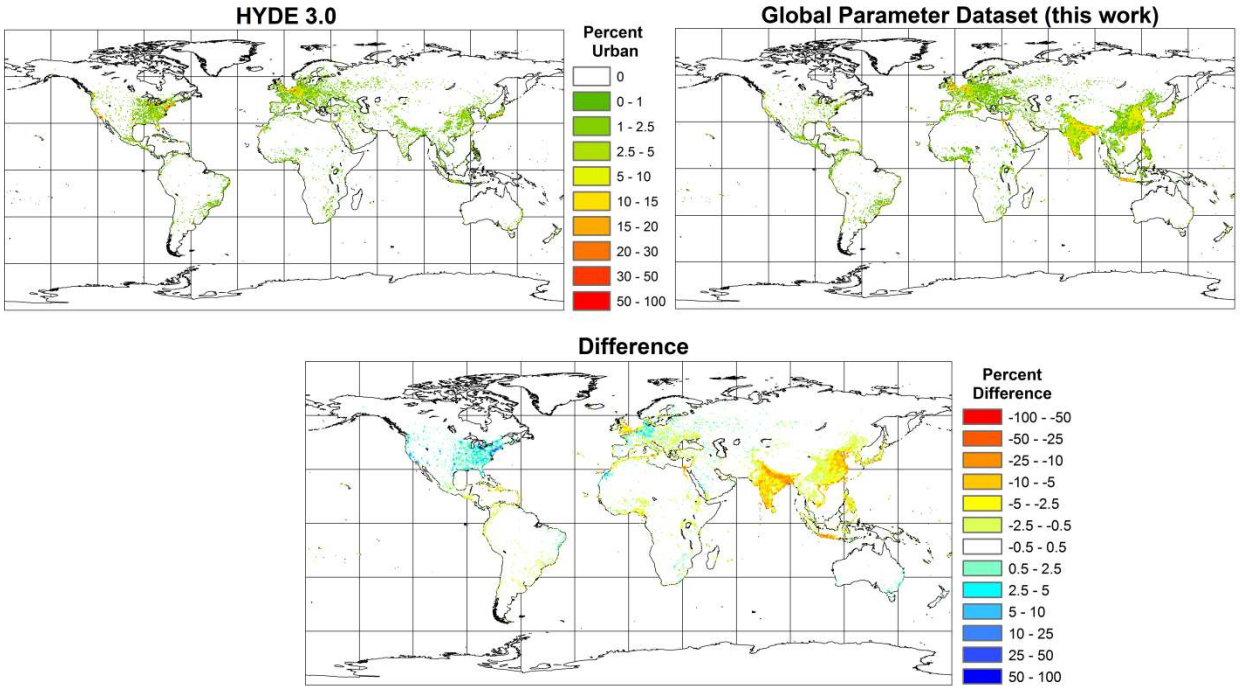

Figure 7. Comparison with the summed TBD, HD and MD urban extent based on this work and the HYDE 3.0 (Klein Goldewijk and van Drecht 2006) urban areas of the world.

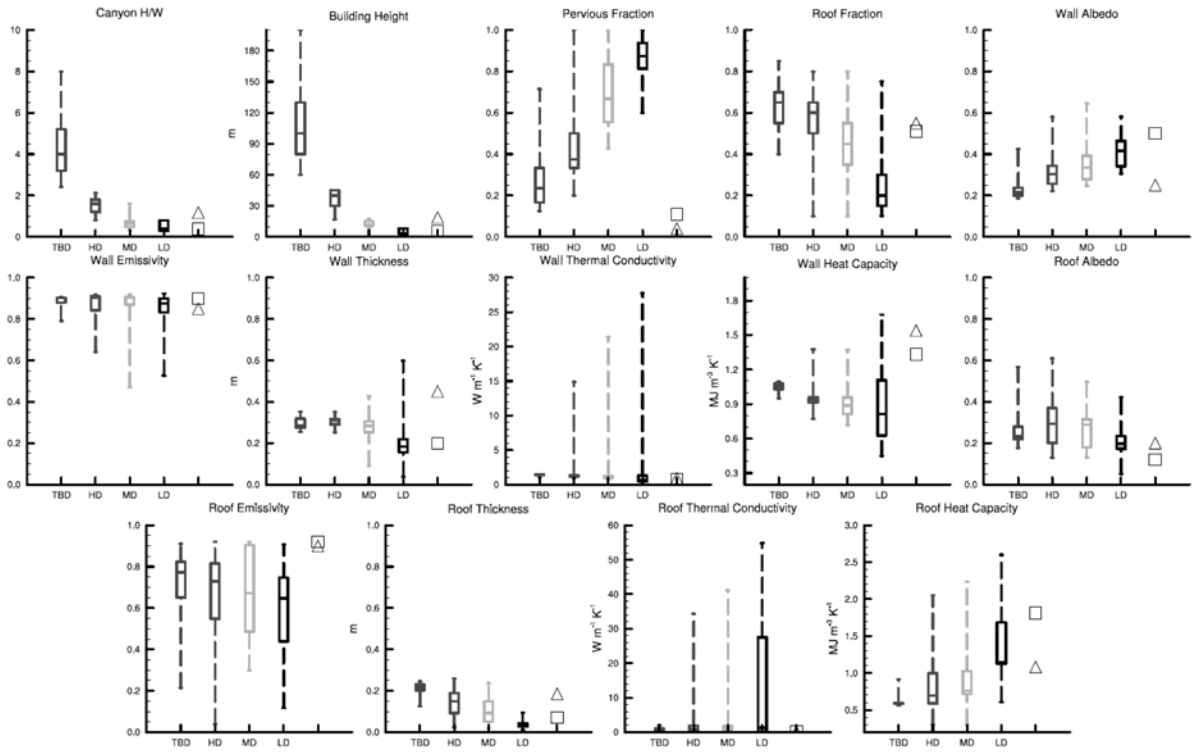

Figure 8. Box plots of parameter values estimated for the 33 regions. For reference, values for Vancouver (open triangles) used in the control experiment (Voogt and Grimmond 2000) and Mexico City (open squares) are also included (Jauregui 1986).

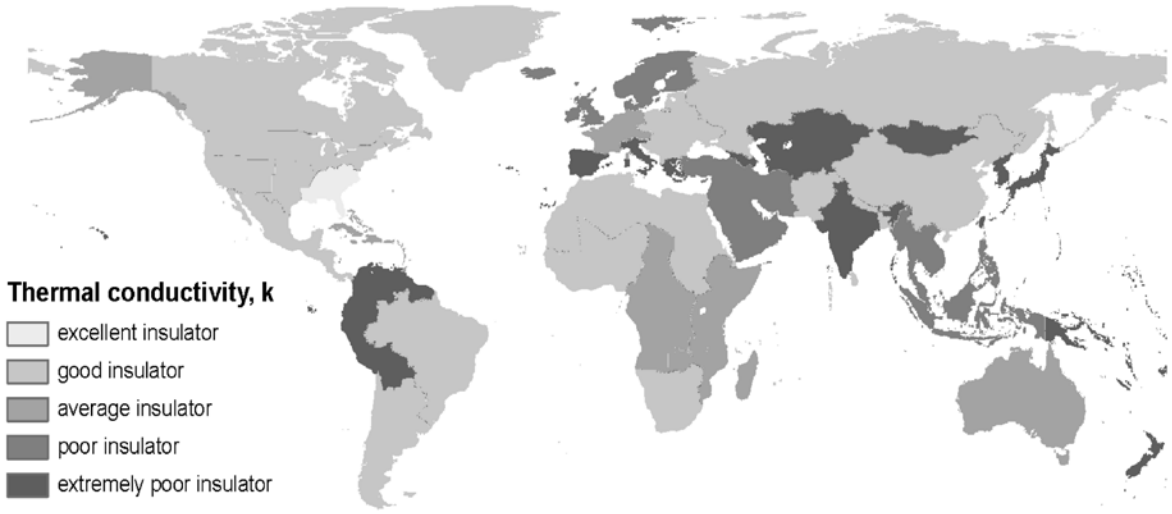

Figure 9. Thermal efficiency of typical walls in medium density category by region. Insulator rankings are based on thermal conductivity values ranging from 0.7 to 3.1 $Wm^{-1}K^{-1}$.

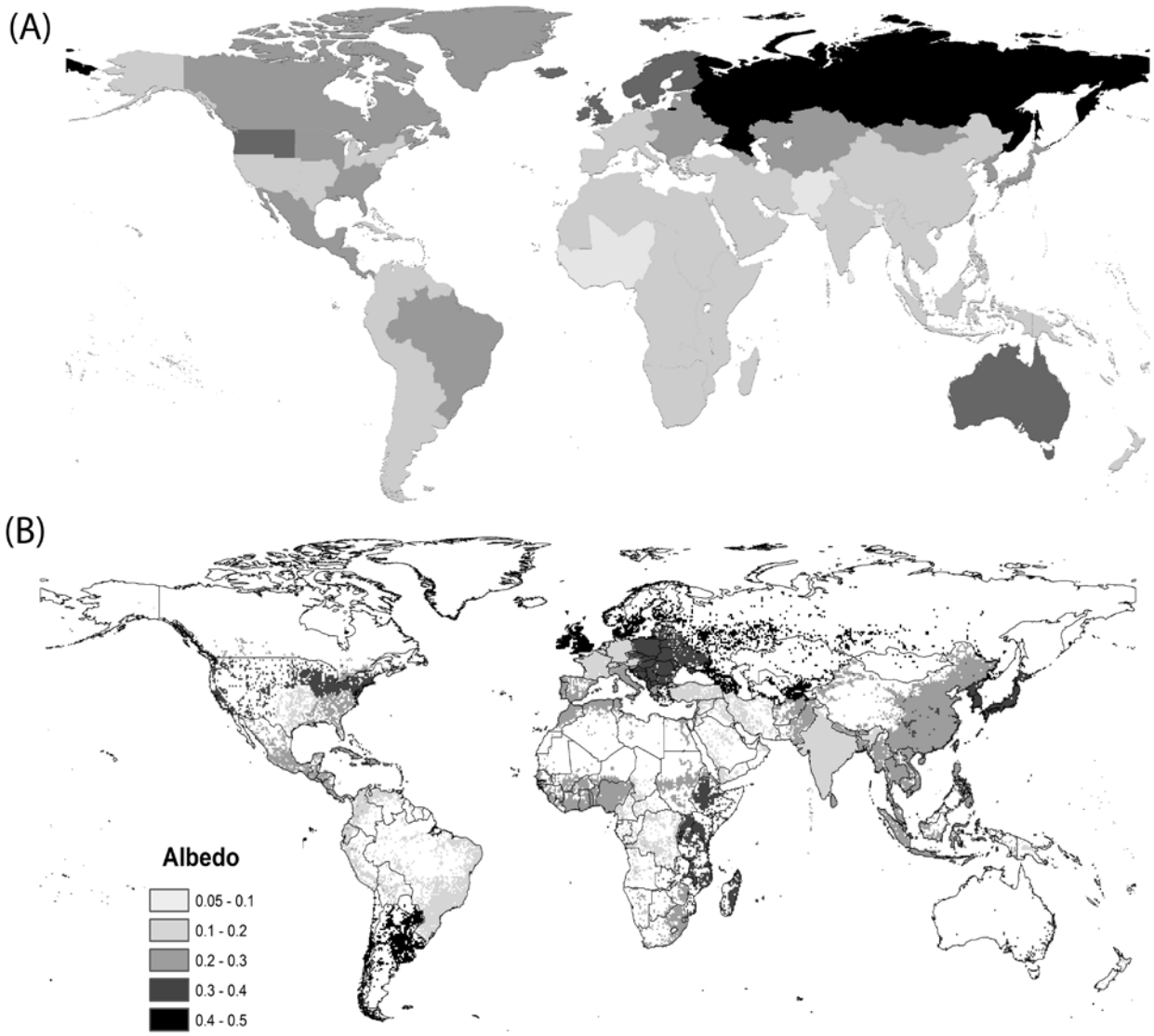

Figure 10. A) Albedo of typical roof materials used in low density category by region, and B) Roof albedo values as actually used in the CLM experimental simulation based on the dominant urban type in a GCM grid cell.

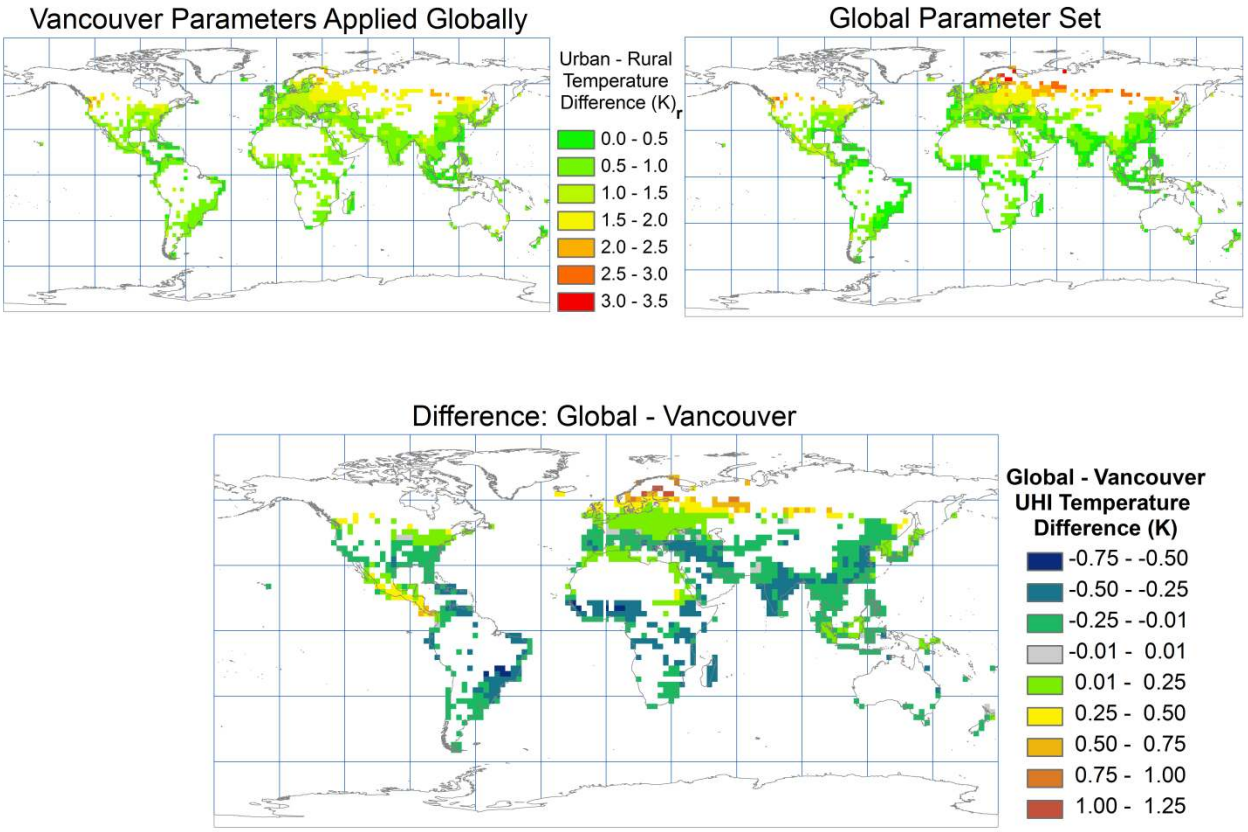

Figure 11. Comparison of simulations assuming all urban areas have the properties of the Voogt and Grimmond (2000) Vancouver location versus simulations using the new parameter dataset.

References

Arnfield, A. J. 1984. Simulating radiative energy budgets within the urban canopy layer. *Modeling and Simulation* 15:227-233.

———. 2000. A simple model of urban canyon energy budget and its validation. *Physical Geography* 11:220-239.

———. 2003. Two decades of urban climate research: A review of turbulence, exchanges of energy and water, and the urban heat island. *International Journal of Climatology* 23:1-26.

Anandakumar, K. 1999. A study on the partition of net radiation into heat fluxes on a dry asphalt surface. *Atmospheric Environment* 33:3911-3918.

Asaeda, T., V. T. Ca, and A. Wake. 1996. Heat storage of pavement and its effect on the lower atmosphere. *Atmospheric Environment* 30:413-427.

Bonan, G. 2002. *Ecological Climatology: Concepts and Applications*. Cambridge, MA: Cambridge University Press.

Center for International Earth Science Information Network (CIESIN), Columbia University; International Food Policy Research Institute (IPFRI), the World Bank; and Centro Internacional de Agricultura Tropical (CIAT). 2004. *Global Rural-Urban Mapping Project (GRUMP): Urban Extents*. Palisades: CIESIN, Columbia University. http://beta.sedac.ciesin.columbia.edu/gpw. (last accessed 17 July 2009).

Changnon, S. A. 1992. Inadvertent weather modification in urban areas: Lessons for global climate change. *Bulletin of the American Meteorological Society* 73:619–627.

Cionco, R. M. and R. Ellefsen. 1998. High resolution urban morphology data for urban wind flow modeling. *Atmospheric Environment* 32:7-17.

Clarke, D., ed. 1989. *Approaches to the study of traditional dwellings and settlements.* Berkeley: Center for Environmental Design Research, University of California at Berkeley.

Collins, W. D., C. M. Bitz, M. L. Blackmon, G. B. Bonan, C. S. Bretherton, J. A. Carton, P. Chang, S. C. Doney, J. J. Hack, T. B. Henderson, J. T. Kiehl, W. G. Large, D. S. McKenna, B. D. Santer, and R. D. Smith. 2006. The Community Climate System Model: CCSM3. *Journal of Climate* 19:2122-2143.

Decker, E. H., S. Elliott, F. A. Smith, D. R. Blake, and F. S. Rowland. 2000. Energy and material flow through the urban ecosystem. *Annual Review of Energy and the Environment* 25:685–740.

DigitalGlobe. 2007. *FAQ.* http://www.digitalglobe.com/index.php/16/About+Us. (last accessed 17 July 2009).

Dobson, J. E., E. A. Bright, P. R. Coleman, R. C. Durfee, and B. A. Worley. 2000. LandScan: A global population database for estimating populations at risk. *Photogrammetric Engineering and Remote Sensing* 66 (7):849-857.

Doll, D., J. K. S. Ching and J. Kaneshiro. 1985. Parameterization of subsurface heating for soil and concrete using net radiation data. *Boundary-LayerMeteorology* 32:351-372.

EarthSat. 2007. MDA EarthSat Satellite Imagery. http://www.earthsat.com/. (last accessed 17 July 2009).

Ellefsen, R. 1990-91. Mapping and measuring buildings in the canopy boundary layer in ten U.S. cities. *Energy and Buildings* 15-16:1025-1049.

Emporis Corporation. 2007. Emporis Buildings - The Building Industry Platform. http://www.emporis.com/en/. (last accessed 17 July 2009).

Environmental Protection Agency (EPA). 2009. Urban Heat Islands: Cool Roofs.

http://www.epa.gov/hiri/mitigation/coolroofs.htm (last accessed 17 July 2009).
Givoni, B. 1976. *Man Climate and Architecture*, 2nd ed. London: Applied Science Publishers.
Klein Goldewijk, K. and G. van Drecht. 2006. HYDE 3: Current and historical population and land cover. ed., A.F. Bouwman, T. Kram and K. Klein Goldewijk. *Integrated modelling of global environmental change. An overview of IMAGE 2.4.* Bilthoven, The Netherlands: Netherlands Environmental Assessment Agency (MNP).
Grimmond, C. S. B. 2007. Urbanization and global environmental change: local effects of urban warming. *The Geographical Journal* 173:83-88.
Grimmond, C. S. B., H. A. Cleugh, and T. R. Oke. 1991. An objective urban heat storage model and its comparison with other schemes. *Atmospheric Environment* 25B:311-326.
Grimmond, C. S. B. and T. R. Oke. 1999. Heat storage in urban areas: Local-scale observations and evaluation of a simple model. *Journal of Applied Meteorology* 4(7):922-940.
Grimmond, C. S. B and C. Souch. 1994. Surface description for urban climate studies: a GIS based methodology. *Geocarto International* 1:47-59.
Grimmond, C. S. B., C. Souch, and M. D. Hubble. 1996. Influence of tree cover on summertime surface energy balance fluxes, San Gabriel Valley, Los Angeles. *Climate Research* 6:45-57.
Howard, L. 1833. *Climate of London deduced from meteorological observations*, Vol. 1-3. London: Harvey and Darton.
Jackson, T. 2007. *Developing a dataset for simulating urban climate impacts on a global scale*. Master's thesis, Department of Geography, University of Kansas, Lawrence.
Jauregui, E. 1986. The urban climate of Mexico City. In: Oke, T. R., ed. Proceedings WMO Technology Conference (Tech Note 652:63–86), Geneva
Kjelgren, R. and T. Montague. 1998. Urban tree transpiration over turf and asphalt surfaces. *Atmospheric Environment* 32:35-41.
Landsberg, H. E. 1981. *The Urban Climate.* New York: Academic Press.
Masson, V. 2000. A physically-based scheme for the urban energy budget in atmospheric models. *Boundary-Layer Meteorology* 94:357-397.
Mills, G. M. 1993. Simulation of the energy budget of an urban canyon – I. Model structure and sensitivity test. *Atmospheric Environment B* 27:157-170.
Mills, G. 2007. Cities as agents of global change. *International Journal of Climatology* 27:1849-1857.
Oak Ridge National Laboratories (ORNL). 2005. LandScan™ 2004 Global Population Database. Oak Ridge National Laboratory, Oak Ridge, TN. http://www.ornl.gov/landscan/. (last accessed 17 July 2009).
Oke, T. R. 1974. *Review of urban climatology, 1968-1973*. Technical Note 134 (publication No. 383). Geneva: World Meteorological Organization.
———1979. *Review of Urban Climatology, 1973-1976.* Technical Note 169 (publication No. 539). Geneva: World Meteorological Organization.
———1982. The energetic basis of the urban heat island. *Quarterly Journal of the Royal Meteorology Society* 108:1-24.
———1987. *Boundary Layer Climates*. 2nd ed. New York: Methuen & Co.
———1988. The urban energy balance. *Progress in Physical Geography* 12:471-508.
———1989. The micrometeorology of the urban forest. *Philosophical Transactions of the Royal Society of London, Series B* 324:335-349.

———1995: The heat island characteristics of the urban boundary layer: Characteristics, causes and effects. *Wind Climate in Cities*, eds. J. E. Cermak, A. G. Davenport, E. J. Plate, and D. X. Viegas, 81–107. Netherlands: Kluwer Academic.

Oke, T. R., G. T. Johnson, D. G. Steyn, and I. D. Watson. 1991. Simulation of surface urban heat islands under "ideal" conditions at night, part 2: diagnosis of causation. *Boundary-Layer Meteorology* 56:339-358.

Oleson, K.W., Y. Dai et al. 2004. *Technical description of the Community Land Model (CLM)*, NCAR Technical Note NCAR/TN-461+STR.

Oleson, K., G. Bonan, and J. Feddema. 2006. Development of an urban parameterization for a global climate model. Presentation for the American Meteorological Society annual meeting, 2006.

Oleson, K. W., G. B. Bonan, J. Feddema, M. Vertenstein, and C. S. B. Grimmond. 2008a. An urban parameterization for a global climate model: 1. Formulation and evaluation for two cities. *Journal of Applied Meteorology and Climatology* 47(4):1038-1060.

Oleson, K. W., G. B. Bonan, J. Feddema, M. Vertenstein, and C. S. B. Grimmond. 2008b. An urban parameterization for a global climate model: 2. Sensitivity to input parameters and the simulated urban heat island in offline simulations. *Journal of Applied Meteorology and Climatology* 47(4):1061-1076.

Oleson, K. W., G.-Y. Niu, Z.-L. Yang, D. M. Lawrence, P. E. Thornton, P. J. Lawrence, R. Stockli, R. E. Dickinson, G. B. Bonan, S. Levis, A. Dai, and T. Qian, 2008c. Improvements to the Community Land Model and their impact on the hydrological cycle. *Journal of Geophysical Research* 113:G01021-B01035.

Oleson, K. W., G. B. Bonan, and J. J. Feddema. 2010. The effects of white roofs on the global urban heat island. *Geophysical Research Letters* 37: L03701.

Oleson, K. W., G. Bonan, J. Feddema, and T. Jackson. An examination of urban heat island characteristics in a global climate model. Forthcoming: *International Journal of Climatology.*

Olgyay, V. 1992. *Design with Climate.* New York: Van Nostrand Reinhold.

Paterson, D. A. and C. J. Apelt. 1989. Simulation of wind flow around three-dimensional buildings. *Building and Environment* 24:39-50.

Qian, T., A. Dai, K. E. Trenberth, K. W. Oleson. 2006. Simulation of global land surface conditions from 1948 to 2004: Part I: Forcing data and evaluations. *Journal of Hydrometerology* 7:953-975.

Rashkin, S., R. A. G. Chinery, (U.S. EPA ENERGY STAR for Homes), D. Melsegeler, D. Gamble (ICF International). 2008. *Technology adoption plan: Advanced New Home Construction.* http://www.epa.gov/cppd/climatechoice/Adv%20New%20Home%20Constr%20Adopt%20Plan3.pdf (last accessed 17 July 2009).

Salhani, P. 2009. Go green with style. *The Sydney Morning Herald.* 18 July 2009.

Schneider, A., M. A. Friedl, D. Potere. 2009. A new map of global urban extent from MODIS satellite data. *Environmental Research Letters* 4:1-11.

Shepherd, J. M. 2005. A review of current investigations of urban-induced rainfall and recommendations for the future. *Earth Interactions* 9:1-27.

Straube, J. F. and E. F. P. Burnett. 2005. *Building Science for Building Enclosures.* Westford: Building Science Press, Inc.

Suckling, P. W. 1980. The energy balance microclimate of a suburban lawn. *Journal of Applied*

Meteorology 19:606-608.
Terjung, W. H. and P. A. O'Rourke. 1980a. Simulating the causal elements of urban heat islands. *Boundary-Layer Meteorology* 19:93-118.
Terjung, W. H. and P. A. O'Rourke. 1980b. Influences of physical structures on urban energy budgets. *Boundary-Layer Meteorology* 19:421-439.
Verseghy, D. L. and D. S. Munro. 1989a. Sensitivity studies on the calculation of the radiation balance of urban surfaces: I. Shortwave radiation. *Boundary-Layer Meteorology* 46:309-331.
Verseghy, D. L. and D. S. Munro. 1989b. Sensitivity studies on the calculation of the radiation balance of urban surfaces: II. Longwave radiation. *Boundary-Layer Meteorology* 46:309-331.
Voogt, J. A., and C. S. B. Grimmond. 2000. Modeling surface sensible heat flux using surface radiative temperatures in a simple urban area. *Journal of Applied Meteorology* 39:1679-1699.

Correspondence: Department of Geography, University of Kansas, Lawrence, KS 66045, email: trish@ku.edu (Jackson), feddema@ku.edu (Feddema); National Center for Atmospheric Research, Climate and Global Dynamics Division, P.O. Box 3000, Boulder, CO 80307, email: oleson@ucar.edu (Oleson), bonan@ucar.edu (Bonan); Department of Geography, University of Nebraska – Kearney, Kearney, NE 68849, email: bauerjt@unk.edu (Bauer).